11th World Congress on Computational Mechanics (WCCM XI)
5th European Conference on Computational Mechanics (ECCM V)
6th European Conference on Computational Fluid Dynamics (ECFD VI)
E. Oñate, J. Oliver and A. Huerta (Eds)

MESH DEFORMATION TOOL FOR OFFSHORE WIND TURBINES FLUID-STRUCTURE INTERACTION

S.G.Horcas*, F.Debrabandere[1], B.Tartinville[1], Ch.Hirsch[1] and G.Coussement[2]

[*,1] NUMECA International
189 Ch. de la Hulpe, B-1170 Bruxelles, Belgium
e-mail: sergio.gonzalez@numeca.be, web page: www.numeca.be

[2] University of Mons, Faculty of Engineering, Fluids-Machines Department
53 rue du Joncquois, B-7000 Mons, Belgium

Key Words: Computational Fluid Dynamics (CFD), Fluid-Structure Interaction (FSI), Mesh deformation, Offshore Wind Turbine (OWT)

Abstract. This paper will describe a new development aiming to deform multi-block structured viscous meshes during fluid solid interaction simulations. The focus will be put on the deformation of external aerodynamic configurations accounting for large structural displacements and 3D multimillion cells meshes. In order to preserve the quality of the resulting mesh, it was understood as a fictitious continuum during the deformation process. Linear elasticity equations were solved with a multigrid and parallelized solver, assuming a heterogeneous distribution of fictitious material *Young modulus*. In order to improve the efficiency of the system resolution an approximate initial solution was obtained prior to the elastic deformation, based on *Radial Basis Functions* and *Transfinite* interpolators. To validate the performances of the whole algorithm, the DTU 10MW reference offshore wind turbine described by [2] is analyzed.

1 INTRODUCTION

Strong dynamical effects are expected during the whole life cycle of Offshore Wind Turbines (OWTs). The combination of this violent loading scenario and the slenderness of rotor blades requires considering Fluid-Structure Interaction (FSI) effects at the design stage.

Industry standards for OWT aerodynamic loads computations are based on simplified engineering models [7][12]. Even if these numerical approaches are less computationally demanding, three-dimensional flow effects are just estimated based on empirical corrections. Hence, the development of more sophisticated CFD techniques for the detailed design of the rotor is justified as stated by [16].

To account for FSI phenomena, the discretized fluid domain needs to be readapted to structural deformations, motivating the implementation of *mesh deformation algorithms*. We have developed a mesh deformation tool based on the original formulation of the *elastic analogy* described by [10]. The performances of the implemented methodology are compared with other approaches, such as the *Elliptic smoothing*. Special attention was paid to the deformation of complex meshes including tens of million points.

To illustrate the performances of the developed solution in the framework of a complete FSI simulation, the DTU 10-MW Reference Wind Turbine [2] was studied. All presented simulations

were performed with the help of the commercial CFD package FINE^{TM}/Turbo [17]. As a first approach, in order to focus on the study of rotor aeroelastic effects, the tower was not modeled in this preliminary analysis. A reduced-order model (ROM) was chosen for the structure, described by its mode shapes and natural frequencies. Steady FSI simulations at different operating points were performed, in order to quantify the expected deformations of the rotor.

2 METHODOLOGY

The commercial package FINE^{TM}/Turbo is used for this study. The flow solver is a three-dimensional, density-based, structured, multi-block Navier-Stokes code using a finite volume method. Central-difference space discretization is employed for the spatial discretization with Jameson type artificial dissipation. A four-stage explicit Runge-Kutta scheme is applied for the temporal discretization. Multi-grid method, local time-stepping and implicit residual smoothing are used in order to speed-up the convergence. Unsteady computations are performed using a dual time stepping approach [9] .For FSI applications, the CFD computational domain deforms according to the solid displacement. Additionally, it requires the resolution of Arbitrary Lagrangian-Eulerian (ALE) formulation of the Navier-Stokes equations [5].

The structure is represented by its natural frequencies and mode shapes. These are determined outside the flow solver and prior to any CFD computation, either by computation with a FEM structure solver or by experiments. Using these structural properties, the elastic body deformation under the action of the fluid loads is computed by a structural solver integrated inside the flow solver [5].

As the mode shapes are defined on a Finite Element mesh, some interpolation issues between structure and fluid data may occur [6]. In order to avoid this, mode shapes are interpolated onto the fluid mesh prior to the coupled computation as suggested by [18]. A RBF interpolation method is also used for this purpose.

3 MESH DEFORMATION METHODS OVERVIEW

Several mesh deformation tools are already available in the described code. In particular, a point-by-point scheme based on *Radial Basis Function* (RBF) interpolation developed by [4] has been proved as a robust and high quality tool for a wide variety of applications. However, this method is limited by its scalability. In fact, the cost of calculation of the interpolation coefficients scales with $O(n_b^3)$ and the new coordinates evaluation with $O(n_b n_i)$, where n_i is the number of inner mesh nodes and n_b is the number of boundary nodes. The reason why it is hardly applicable to multimillion 3D meshes.

In order to develop a fast and robust method for big OWT rotor blades mesh deformation, a *connectivity-based* approach was chosen from the very beginning. In this line, a popular and simple technique is the so called *Elliptic smoothing*, which was implemented in the considered code prior this research [17]. With this method, new mesh nodes position is calculated by solving the linear system:

$$\vec{\nabla}(\omega\vec{\nabla}(\vec{x}-\vec{x}_{ref}))=0 \tag{1}$$

Where x is the position of the mesh node, x_{ref} the position corresponding to the undeformed mesh and ω a local diffusivity factor aiming to preserve the final mesh quality by limiting the deformation of small volume cells.

Even if the diffusivity is controlled by ω, the limitations of the *Elliptic smoothing* when dealing

with large displacements have been extensively described in the literature [8][13][1]. In particular, mesh folding is often observed around concave regions as illustrated in Figure 1, corresponding to the deformation of a 2D vortex induced vibrations test case [19]:

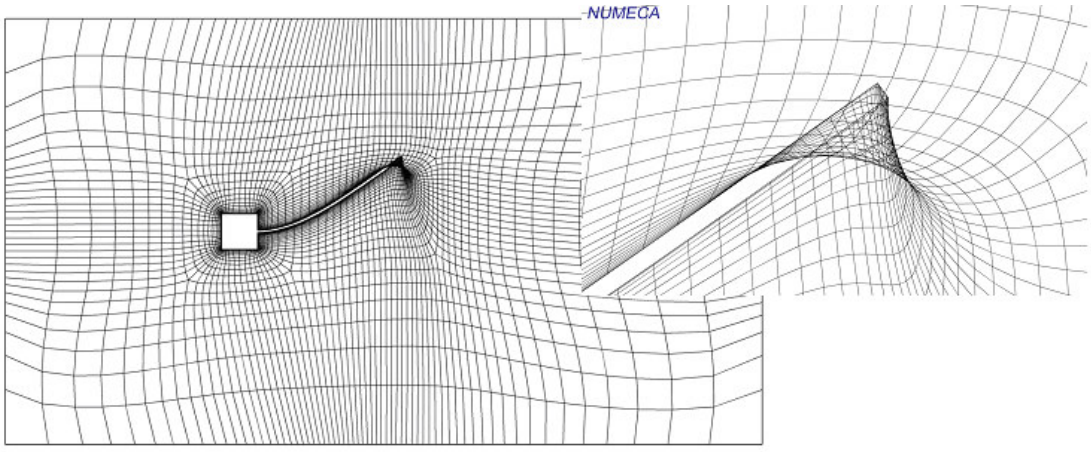

Figure 1: Vortex Induced Vibrations 2D Test Case, elliptic smoothing deformation

The new developed algorithm is based on the *Elastic Analogy* [10]. In this case, the diffusion mechanism is controlled by considering the CFD mesh as an elastic continuum. A finite volume discretization has been coded in order to reproduce the elastic equations of our fictitious material:

$$\iint_S \left(\lambda(\nabla \cdot \vec{x})\overline{\overline{I_3}} + \mu\left((\nabla\vec{x})^t + \nabla\vec{x}\right)\right) \cdot \vec{n} dS = 0 \tag{2}$$

Where λ and μ correspond to the so called *Lame Coefficients* and can be directly related to the elastic properties (*Young Modulus* and *Poisson Ratio*) given to our continuum:

$$\mu = \frac{E}{2(1+\nu)} \tag{3}$$

$$\lambda = \frac{\nu E}{(1+\nu)(1-2\nu)}$$

In order to control the orthogonality of our mesh near the walls and its overall quality, a heterogeneous distribution of the elastic properties is needed [22][21]. A good resulting mesh quality can be then obtained for the considered 2D example, Figure 2.

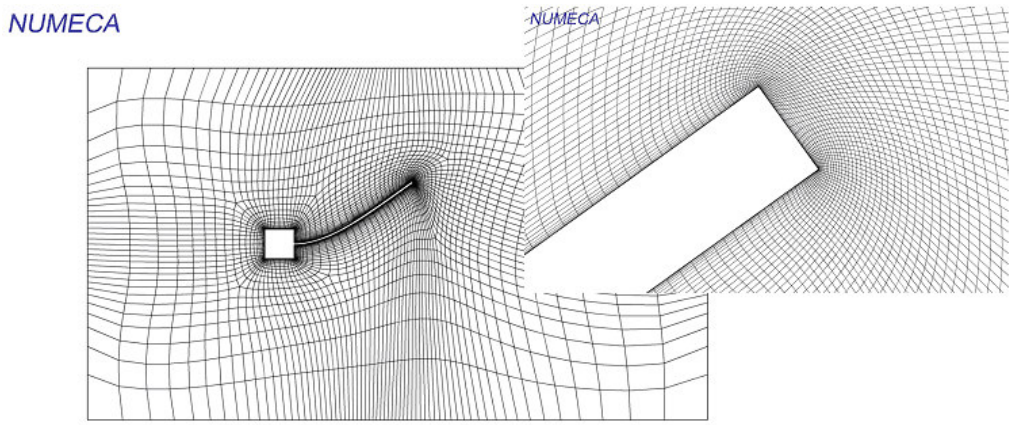

Figure 2: Vortex Induced Vibrations 2D Test Case, elastic analogy deformation

In the framework of structured meshes, a very interesting tool to be used in mesh deformation is the *Transfinite Interpolation* (TFI). This method can not be considered as a mesh deformation technique by its own (since it needs as an INPUT the displacements of our blocking topology). However, its reduced computational time makes it very attractive as an intermediate or final step in the complete mesh deformation process.

The arc-length based TFI method suggested by [14] has been implemented for this purposes. Let us consider a mesh segment going from point A to B. Then we can define the arc-length of an interior point *i* as:

$$l_i = \left| \vec{x}_{ref,i} - \vec{x}_{ref,i-1} \right| \tag{4}$$

And the total arc-length of the segment as:

$$L_{BA} = \sum_{i=A+1}^{B} \left| \vec{x}_{ref,i} - \vec{x}_{ref,i-1} \right| \tag{5}$$

Then, new edge interior points coordinates can be computed by performing a linear interpolation:

$$x_i - x_{ref,i} = \left[1 - \frac{l_i}{L_{BA}} \right] \left(x_A - x_{ref,A} \right) + \left[\frac{l_i}{L_{BA}} \right] \left(x_B - x_{ref,B} \right) \tag{6}$$

As performed by [14], this 1D interpolation can be easily extrapolated to a 2D version for block surface interpolation or to 3D for block interior nodes recomputation. The combination of these 1D/2D/3D interpolators allows then to remap our blocks starting either from the deformed position of block corners, edges or faces.

4 VALIDATION TEST CASE, AERODYNAMIC SIMULATIONS

For the validation of the presented aeroelastic prediction methodology, the reference wind turbine described by [2] at different working points was analyzed, assuming a steady flow behavior.

First aerodynamic simulations were performed in order to validate our CFD case set-up with respect to the available literature references. CFD RANS simulations at different 0 deg. pitch operating points were carried out for this purpose.

4.1 Mesh generation

In order to build a 3D mesh of the DTU 10MW wind turbine, blade sections were imported in AUTOGRID™ 5 from data published by [2]. Blade surfaces at 0 deg. pitch, as well as nacelle and hub geometries were included in this process.

A blocking topology was established around the blade (Figure 3), putting a special attention in the local mesh around the blunt edge and blade tip.

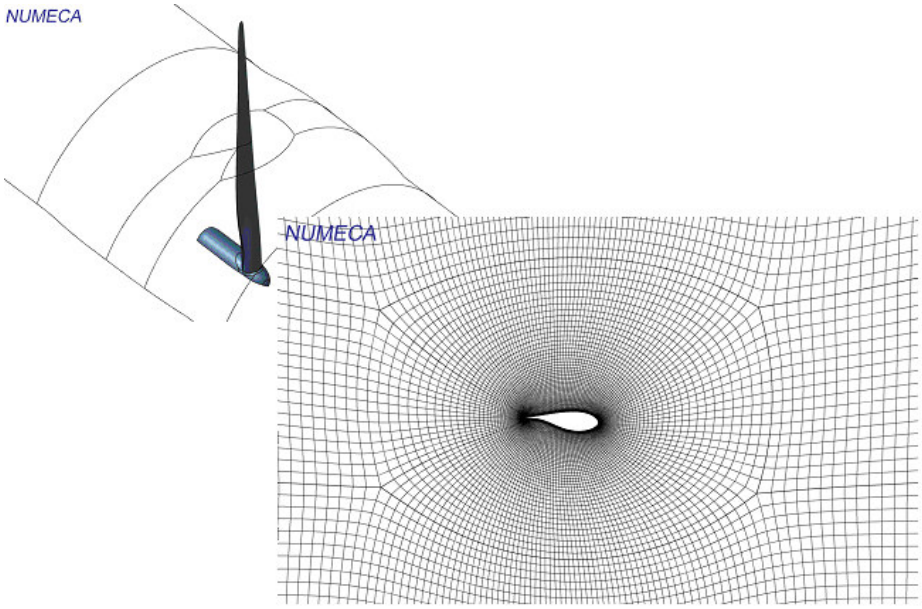

Figure 3: Detail of mesh at a mid-span cut

A $7.24 \cdot 10^6$ nodes mesh was obtained, accounting for 4 grid levels and 24 blocks.

4.2 CFD Results

First CFD simulation aimed to analyze the nominal operating point of the DTU 10 MW reference wind turbine in a rigid rotor configuration:

- Rotational speed: 8.836 RPM
- Incoming wind speed: 11 m/s
- Pitch angle: 0 deg.

A Spallart-Allmaras turbulence model was used for our RANS simulation, enhanced by Merkle preconditioner. A multigrid approach was followed in order to speed-up our computations, which were launched in parallel.

Obtained global thrust and mechanical power were in agreement with the results already published by [2]. The span evolution of the local thrust and power coefficients defined by [11] were also fitting the considered literature reference, where 3D RANS simulations were performed with ELLIPSYS 3D.

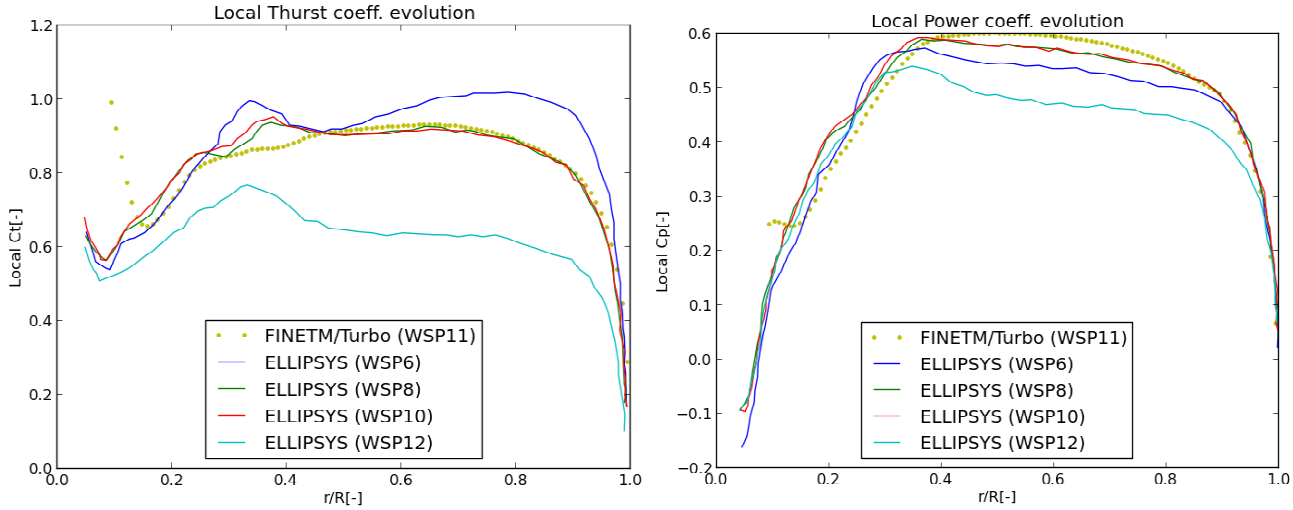

Figure 4: Local Thrust and Power coefficient evolution along blade span

The increase of local thrust and power observed at span values lower than 30% is related to the differences in modeled blade geometries for both CFD solvers simulations. Indeed, all simulations carried out by the authors of this paper considered a blade equipped with *Gurney flaps* for low span blade profiles. For the case of ELLIPSYS 3D reference values, the *straight blade* detailed in [2] was modeled. The observed increase in local coefficients is then in line with the already performed comparisons during DTU 10 MW blade design stage [3]. From the local flow point of view, huge recirculations were observed near blade trailing edges at the span range were the *Gurney flaps* are equipped [20%, 30%], due to the violent profiles curvature (Figure 5).

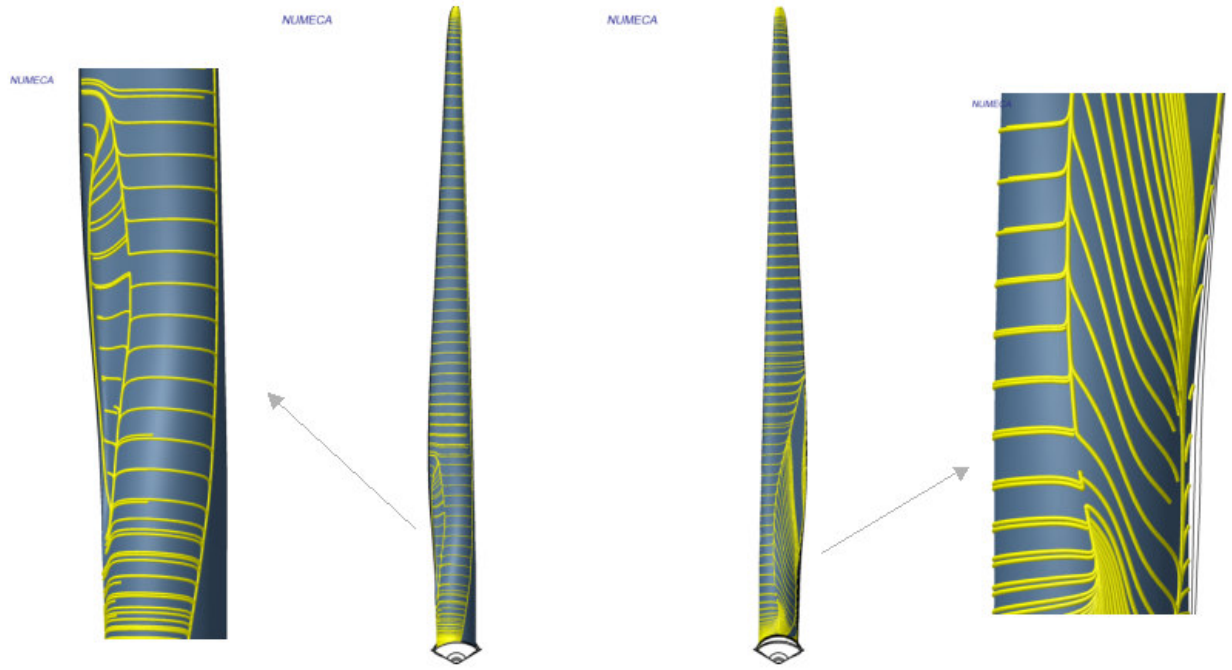

Figure 5: Blade streamlines at nominal operating point, pressure (left) and suction (right) sides

In addition to this huge 3D turbulent structures along the blade span, the tip vortex was identified as an important local flow effect.

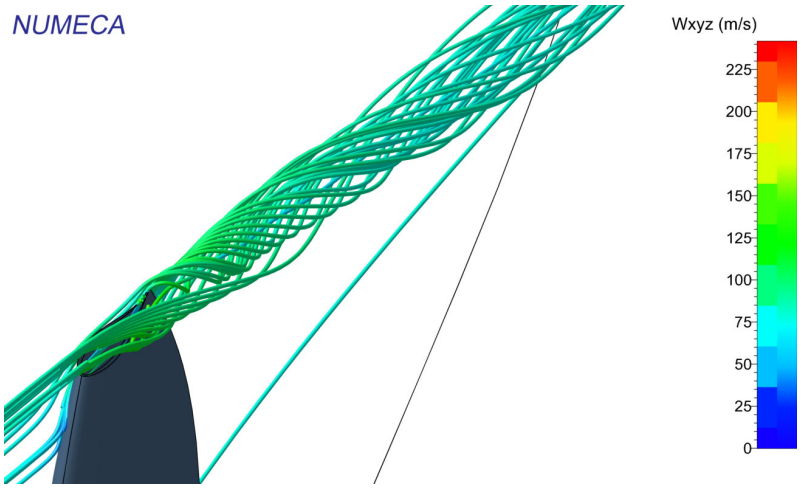

Figure 6: Blade tip streamlines at nominal point

In order to extend the validation of our flow set-up, different operating points of the DTU 10MW wind turbine at 0 deg. pitch were also analyzed (Table 1). A good agreement in terms of total thrust and power with respect to [2] was obtained. Global thrust and power results are shown in Figure 7.

Table 1: DTU 10MW aerodynamic load cases definition

DLC Identifier	Wind Speed (m/s)	R.P.M.
FT_WSP07	7	6.000
FT_WSP08	8	6.426
FT_WSP09	9	7.229
FT_WSP10	10	8.032
FT_WSP11	11	8.836

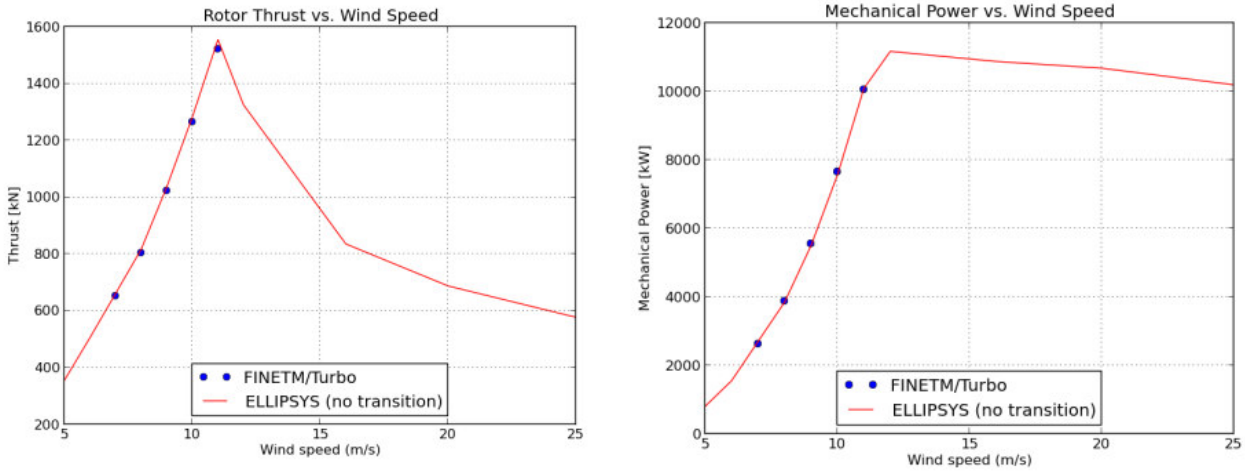

Figure 7: Global Thrust and Power versus wind speed

In addition, the expected local power and thrust coefficients evolution was observed.

4 VALIDATION TEST CASE, AEROELASTICITY PREDICTION

A steady aeroelastic simulation was performed starting from the already described CFD computation at the nominal operating point of the DTU 10MW reference wind turbine. The behavior of the structure was linearized by means of its natural frequencies and deformed shapes. An iterative procedure *fluid simulation/structure deformation* allowed us to find the final deformed blade and flow behavior after several steps.

4.1 Structural model

For the considered aeroelastic simulations, the structured was linearized by means of the reduced-order model (ROM) developed by [5].

A modal analysis was performed within the commercial package Abaqus [20], thanks to the model provided by [2]. Centrifugal effects were included in this computation in order to take into account their impact on blade stiffness and blade deformation at the considered rotational speed.

Obtained natural frequencies were compared against the aeroelastic computations obtained with Hawc2 [15],a third party software based on blade element momentum theory (BEM). Computed frequencies for each identified mode are compiled in Table 2.

Table 2: DTU 10MW blade modes

Natural Frequency (Hz)		Isolated blade modes	
Abaqus	Bak et al. (2013)	Identifier	Description
0.64	0.61	1	1st flap
0.97	0.93	2	1st edge
1.79	1.74	3	2nd flap
2.89	2.76	4	2nd edge
3.61	3.57	5	3rd flap
5.72	5.69	6	1st torsion
5.77	-	7	Mixed flap/torsion
6.18	6.11	8	4th flap
-	6.66	9	3rd edge

A mixed mode was found between 1st torsion and 4th flap. No pure 3rd edge mode was identified within the considered frequency range. These differences could be explained by the complexity of the structural models used for natural frequencies extraction. As it will be shown later on in this document, the already mentioned dissenting modes did not have an important impact on blade deformation for the considered load case.

4.2 Mesh deformation

A finite volume based version of the *Elastic Analogy* was used as the main mesh deformation technique for this challenging case. An under relaxed Jacobi solver was implemented and parallelized in order to efficiently solve our linear system. A V-cycle multigrid strategy was set-up, allowing us to reduce the computational time by accessing coarser grid levels of our mesh.

To increase the efficiency of our system resolution, a good initial solution was provided by means of a mix of other mesh deformation algorithms. The implemented procedure can be summarized as:

1) Interpolation of block corners *via* a *light RBFI*: Boundary nodes displacements serve as a

base of the interpolation of mesh block corners. A coarsening is applied to the set of boundary nodes in order to speed-up this preliminary stage [5].

2) Block edges and block faces are computed based on *TFI*, in order to have a complete approximate mesh before solving our linear system.
3) *Elastic analogy*: Interior block nodes are then computed by means of an elastic analogy based on the reference mesh. A Young modulus based on each cell wall distance was used. The *Poisson Ratio* of the fictitious material was set to 0.25

4.3 Fluid Solid Interaction Results

A 900 fluid iterations simulation was performed. The structure deformation is first calculated at the beginning of the computation. Then it is updated twice during the computation at iterations 300 and 600 according to the fluid load evolution. Figure 8 shows that the computed global thrust is stabilized even after the second deformation (which does not considerably modify our blade shape). Obtained results matched with the trend already established by [2], since the computed thrust is considerably lower when aeroelastic effects are taken into account. The resulting blade deformation is mainly dominated by mode 1 (1st flap), which was something to expect given the studied load case (Figure 9).

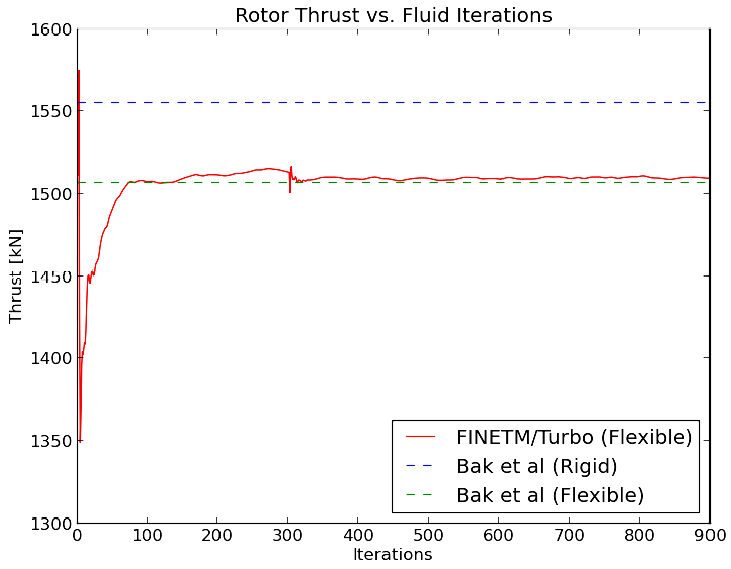

Figure 8: Thrust evolution during aeroelastic simulation at nominal point

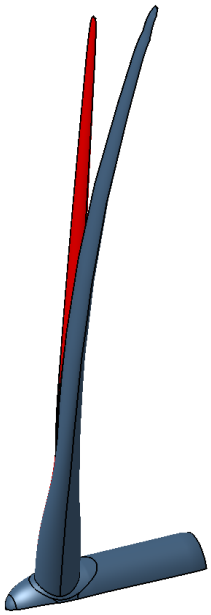

Figure 9: Deformed (blue) and undeformed (red) blade

The deformed mesh at mid-span is comparable with the undeformed one, as shown in Figure 10 and Figure 11.

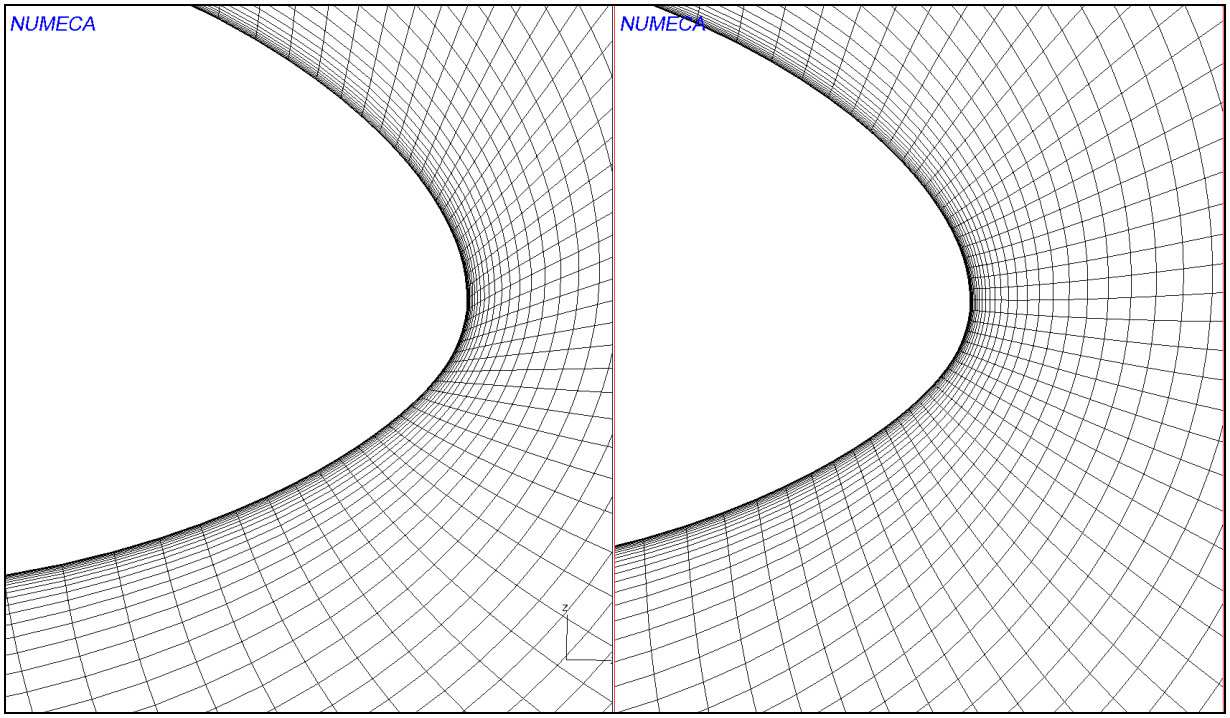

Figure 10: Detail of mid-span leading edge profile for deformed (left) and original (right) meshes

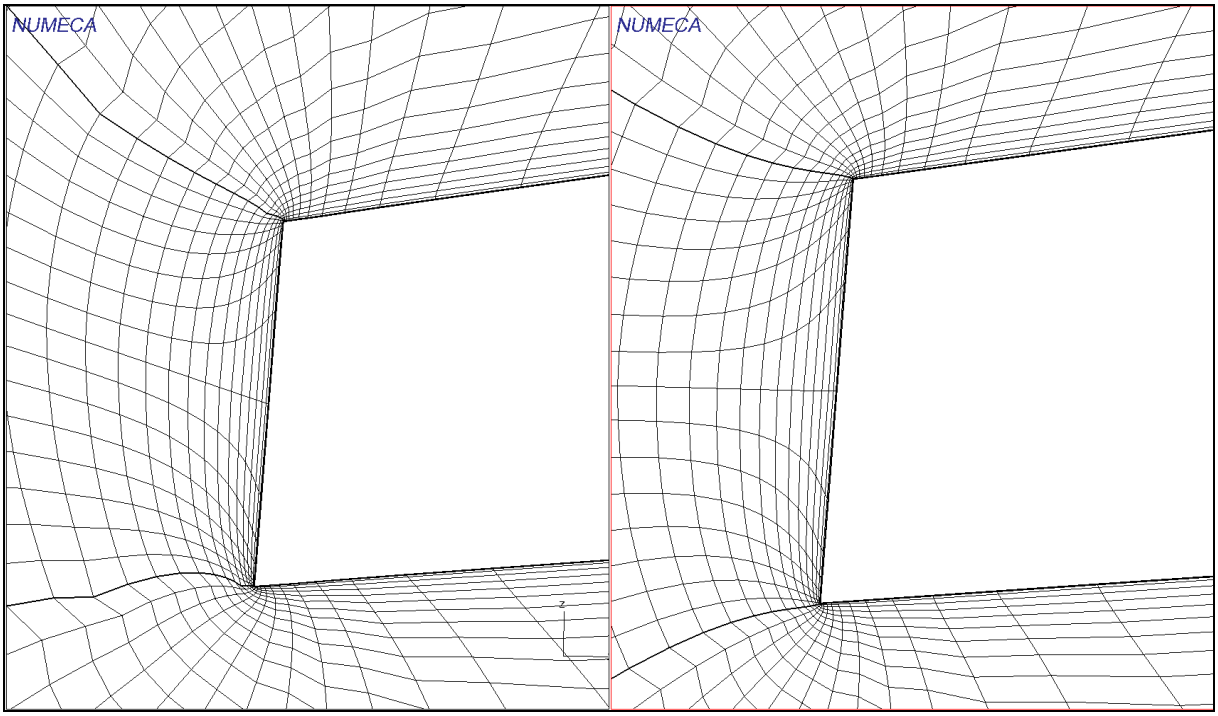

Figure 11: Detail of mid-span trailing edge profile for deformed (left) and original (right) meshes

Globally speaking, only cells aspect ratio is slightly increased after the deformation process in order to accommodate blade deflection (Table 3).

Table 3: Mesh quality of original and deformed DTU 10MW blade mesh

Mesh ID	Orthogonality		Aspect ratio		Expansion ratio	
	Mean value	Standard Deviation	Mean value	Standard Deviation	Mean value	Standard Deviation
Original	77.69	9.78	10805	1005	1.77	0.11
Deformed	77.46	9.98	19250	795	1.79	0.10

The measured out of rotor plane displacement at the blade tip was 7.82 m. Please note that both tilt (5 deg.) and cone (2.25 deg.) angles were not taken into account in our simulation. We can then estimate the tip displacement in our final rotor configuration, 7.74 m, by projecting our deformation.

This displacement implies a margin of 58 % with respect to the tower clearance designed in [2]. As expected, this deformation is lower than the maximum tip deflection measured by the same authors in the Power Production operation DLCs, where it ranges from 10.5 m to 12.4 m. In that analysis a wider variety of incoming wind speeds and directions were taken into account, including near cut-off wind speed configurations.

5 CONCLUSIONS AND FUTURE WORKS

A numerical approach in order to predict aeroelastic effects of multi-megawatt offshore wind turbines rotor has been developed. In particular, a new mesh deformation code based on the *elastic analogy* has been implemented. The performances of the method when dealing with large geometrical deflections have been improved thanks to the coupling with to other complementary approaches: the *transfinite interpolation* (TFI) and the *radial basis function* (RBF).

The efficiency and robustness of the algorithm have been evaluated at the nominal operating point of the DTU 10 MW reference wind turbine. Both aerodynamics and aeroelastic results were successfully checked against previous numerical analyses performed by third party softwares, due to the lack of published experimental data.

Future works will be first devoted to extend the presented rotor flow set-up to unsteady configurations. The actual mesh will be re-built in order to include a DTU 10MW tower model. The interaction between flexible rotor and tower will be then characterized (3P effects). After the consolidation of this unsteady aeroelasticity prediction methodology, the model will serve as a basis for a set of new developments in the code, aiming to account for hydrodynamic excitations on bottom-fixed and floating OWT configurations.

6 AKNOWLEDGMENTS

The authors acknowledge the European Commission (EC) for their research grant under the project FP7-PEOPLE-2012-ITN 309395 “MARE-WINT” (*new MAterials and REliability in offshore WINd Turbines technology*), see: http://marewint.eu/.

REFERENCES

[1] S.Arabi, R.Camarero and F.Guibault, *Unstructured Mesh Motion Using Sliding Cells and Mapping Domains*, 20th Annual Conference of the CFD Society of Canada (2012)

[2] C.Bak, F.Zahle, R.Bitsche, T.Kim, A.Yde, L.C.Henriksen, M.H.Hansen, J.P.A.A.Blasques, M.Gaunaa, A.Natarajan, *The DTU 10-MW Reference Wind Turbine*. Danish Wind Power Research 2013, Fredericia, Denmark (2013). Related data publicly available at http://dtu-10mw-rwt.vindenergi.dtu.dk/

[3] C.Bak, F.Zahle, R.Bitsche, T.Kim, A.Yde, L.C.Henriksen, M.H.Hansen, J.P.A.A.Blasques, M.Gaunaa, N.N.Sorensen, *Developing the basis for the design of a 10 MW lightweight rotor,* Advances in rotor blades for wind turbines (2013)

[4] A.de Boer, M.S. van der Schoot and H. Bijl, *Mesh deformation based on radial basis function interpolation*. Computers and Structures, 85(11-14):784-795 (2007)

[5] F.Debrabandere, *Computational methods for industrial Fluid-Structure Interactions*, PhD Thesis, Universite de Mons (2014)

[6] C. L. Fenwick, C. B. Allen, *Flutter Analysis of the BACT Wing with Consideration of Control Surface Representation*, 25th AIAA Applied Aerodynamics Conference, AIAA 2007-3805. (2007)

[7] A.Heege, A.Gaull, S.G.Horcas, P.Bonnet, M.Defourny, *Experiences in controller adaptations of floating wind turbines through advanced numerical simulations*. AWEA Wind Power Conference. Chicago (2013)

[8] J.Hermansson and P.Hansbo, *A variable diffusion method for mesh smoothing*, Communications in Numerical Methods in Engineering;19:897-908 (2003)

[9] A. Jameson, *Time dependent calculations using multigrid, with applications to unsteady flows past airfoils and wings*, AIAA-Paper 91-1596 (1991)

[10] H. Jasak and H.G.Weller, *Application of the finite volume method and unstructured meshes to linear elasticity*. International Journal for Numerical Methods in Engineering; 48:267-287 (2000)

[11] J.Johansen, H.A.Madsen, N.N.Sorensen, C.Bak, *Numerical Investigation of a Wind Turbine Rotor with an aerodynamically redesigned hub-region* (2007)

[12] J.M.Jonkman, M.L.Buhl Jr., *Development and Verification of a Fully Coupled Simulator for Offshore Wind Turbines*. National Renewable Energy Laboratory (NREL), Conference paper 500-40979 (2007)

[13] S.L.Karman Jr., *Virtual Control Volumes for Two-Dimensional Unstructured Elliptic Smoothing*. Proceedings of the 19th International Meshing Roundatble, IMR, pp.121-142 (2010)

[14] K.L. Lai, H.M. Tsai, *Application of Sploine Matrix for Mesh Deformation with Dynamic Multi-Block Grids*, AIAA-2003-3514 (2003)

[15] T.J. Larsen, A.M. Hansen, *How to HAWC2, the user's manual*, Riso National Laboratory (2007)

[16] Y.Li, K.Paik, T.Xing, P.M.Carrica, *Dynamic overset CFD Simulations of wind turbine aerodynamics*. Renewable Energy, an International Journal. Vol 37, Issue 1:285-289 (2012)

[17] NUMECA International, *FINETM/Turbo v9.0 User Manual*. (2013)

[18] A.I. Sayma, M. Vahdati, M. Imregun, *An Integrated Nonlinear Approach for Turbomachinery Forced Response, Part I: Formulation*, Journal of Fluids and Structures 14, 87–101. (2000)

[19] SCAI, *MpCCI User Manual* v4.2.1. (2012)

[20] DS Simulia, *Abaqus Analysis User's Manual*, Version 6.8 (2008)

[21] K. Stein, T. Tezduyar, R. Benney, *Mesh Moving Techniques for Fluid-Structure Interactions With Large Displacements*, Journal of Applied Mechanics ASME (2003)

[22] Z. Yang, D.J. Mavriplis, *Unstructured Dynamic Meshes with Higher-order Time Integration Schemes for the Unsteady Navier-Stokes Equations*, 4th AIAA Aerospace Sciences Meeting and Exhibit (2005)